Submitted, 2010 American Control Conference (ACC)
http://www.cds.caltech.edu/~murray/papers/zom10-acc_s.html

Experimental Demonstration of the Dynamics and Stability of a Low Reynolds Number Swimmer Near a Plane Wall

Sebastian Zhang, Yizhar Or, and Richard M. Murray

Abstract— **The motion of microorganisms as well as of tiny robotic swimmers for biomedical applications is governed by low Reynolds number (*Re*) hydrodynamics, where viscous effects dominate and inertial effects are negligible. This paper presents experimental results that verify theoretical predictions of our recent work which analyzed the dynamics and stability of a low-*Re* swimmer near a plane wall. The experimental setup uses macro-scale swimmer prototypes which are propelled by rotating cylinders in highly viscous silicone oil. The motion was recorded by a video camera and position measurements were taken by an optical tracking system. The results show good qualitative agreement with our recent theoretical predictions.**

I. Introduction

The motion of microorganisms [1], as well as of tiny robotic swimmers for biomedical applications [2], is governed by low Reynolds number hydrodynamics [3,4]. The Reynolds number, which encompasses the ratio of inertial forces to viscous forces, is defined as $Re=VL/\nu$, where V is a characteristic velocity, L is a characteristic length scale, and ν is the kinematic viscosity of the fluid. For example, a typical Reynolds number for a human swimmer who is governed by inertial effects is in the order of 10^4, whereas a microorganism typically has $Re\approx10^{-3}$ and moves by harnessing viscous effects. In this paper, we report experimental results that verify theoretical predictions of our previous work [5], which analyzed the dynamics and stability of a low-*Re* swimmer near a plane wall.

The theory of low-*Re* swimming has been widely studied in the physics and biology literature [1,3]. In the applicative direction, some efforts to develop miniaturized artificial swimmers were reported, e.g. [2,6-8]. A typical strategy for low-*Re* swimming is to apply cyclic changes in the internal configuration of the swimmer in order to generate net motion [9-11]. It was only recently that this problem has been studied from a control-theoretic viewpoint [12,13]. Earlier works considered geometric-mechanical aspects of swimming in both physics [14,15] and dynamical control systems literature [16-18]. Assuming that the fluid domain is unbounded, these works exploited the geometric structure of the equation of motion, namely the gauge symmetry, in order to formulate the locomotion problem as a connection, or geometric phase, on a principal fiber bundle. However, the presence of solid boundaries destroys the gauge symmetry, and analysis of the physical interaction between the swimmer and the boundary becomes much more complicated to model [19].

Several works have studied wall-swimmer interaction in the context of microorganism motility. Some of them presented numerical simulation results [22,23], and some reported experimental observations [21,24] and suggested simplified theoretical models [20,24]. However, none of these works analyzed the problem from control-theoretic or geometric-mechanical viewpoint. A major step in these directions has been conducted in our recent work [5], which studied the dynamics of low-*Re* swimming near an infinite plane wall for a simple class of articulated swimmers having a constant shape (e.g. [25,26]). In particular, we explicitly analyzed planar motion of swimmers that are comprised of a rigid structure of spheres which are rotated about their axis in order to generate propulsion. We have shown that a swimmer with axisymmetric propulsion, which translates linearly in unbounded fluid, is forced to rotate when put near a plane wall, and is be repelled from the wall along a curved trajectory. When asymmetric propulsion is applied, the swimmer is able to translate steadily parallel to the wall if it possesses fore-aft symmetry. However, when given a perturbation from this steady motion, the swimmer will exhibit neutrally stable periodic motion. When the fore-aft symmetry of the swimmer is broken, it is possible to achieve open-loop asymptotic stability of the parallel translation without requiring sensing or feedback.

The goal of this paper is to verify the theoretical predictions of [5] by presenting results of motion experiments conducted with macro-scale swimmer prototypes in a highly viscous silicone fluid. The swimmers are propelled by rotating cylinders using electric DC motors. Planar motion of the swimmer is enforced by a flotation structure that supports its gravitational load. The motion experiments were recorded by a video camera (movies are available online at [27]), and position measurements were taken using an optical tracking system. The results show good qualitative agreement with the theory in [5] and corroborate our predictions on the physical swimmer-wall interaction.

S. Zhang is with the Mechanical Engineering Department, Clemson University, SC 29634 USA (phone: 864-908-6466; e-mail: sebastz@g.clemson.edu).

Y. Or is with the Mechanical Engineering Department, Technion – Israel Institute of Technology, Haifa 32000, Israel (e-mail: izi@tx.technion.ac.il).

R. M. Murray is with the Control and Dynamical Systems Department, California Institute of Technology, CA 91125 USA, (e-mail: murray@cds.caltech.edu).

This research was supported in part by Boeing Corporation. Y. Or was supported by the Fulbright Postdoctoral Fellowship and the Bikura Postdoctoral Scholarship of the Israeli Science Foundation. This work was performed at the California Institute of Technology.

The structure of the paper is as follows. Section II summarizes the theoretical background presented in [5]. Section III details the experimental methods and the different swimmers used. Section IV presents the experimental results. Section V discusses the results. Conclusions and future work are summarized in section VI.

II. Theoretical Background

We now give background on the theoretical results, based on the analysis in [5]. Consider a simplified model of an articulated micro-swimmer which consists of a collection of n rigid spheres of equal radius a. The spheres are attached to a thin rigid structure, called the *body* of the swimmer. It is assumed that the motion of the swimmer is restricted to the xy plane. The swimmer is submerged in a viscous fluid which is bounded by an infinite solid wall at the plane $y = 0$. The generalized coordinates describing the position and orientation of the swimmer in the plane are denoted $q = (x, y, \theta) \in SO(2)$. Some of the spheres are actuated by rotation about their z-axis which is fixed to the body. The *input* for the swimmer $u \in \Re^m$ is the vector of the angular velocities of all actuated spheres. The simplest example is the *two-sphere swimmer* shown in Fig. 1(a), in which two spheres are connected by a thin rigid rod of length d, and are actuated by angular velocities $u=(u_1,u_2)$. The second example is the 2+1-sphere swimmer shown in Fig. 1(b), in which an additional unactuated sphere is rigidly attached to the swimmer's body. It is shown in [5] that the of motion of the swimmer under given input $u(t)$ is governed by a *driftless nonlinear control system* of the form

$$\dot{q} = G(q)u. \qquad (1)$$

The matrix $G(q)$ (termed *mechanical connection* in the geometric mechanics literature) depends nonlinearly on the configuration q, and encapsulates the geometric structure of the swimmer and the physics of the interaction between the swimmer, the fluid, and the wall.

A. Derivation of the Equation of Motion

We now briefly review the derivation of the swimmer's equation of motion and its geometric properties, as studied in [5]. The Reynolds number governing the motion of the swimmer is assumed to be negligibly small, so that the flow can be described by *Stokes equation* [4], which is the limit of Navier-Stokes equation for the case $Re \to 0$. The boundary conditions are called *no-slip conditions*, and imply that the fluid velocity vanishes on the stationary wall at y=0, and that on the boundaries of the spheres the fluid velocity matches the velocity of the spheres. Let us denote $U = (V_1 \ldots V_n, \omega_1 \ldots \omega_n)$, where $V_i \in \Re^2$ is the linear velocity of the ith sphere center in xy plane, and $\varpi_i \in \Re$ is its angular velocity about the z axis. The linear and angular velocities of the spheres are related to the body velocity $\dot{q}$ and the input velocities u via the linear relation $U = T(\theta)\dot{q} + Eu$, where $T(\theta)$ depends on the geometric arrangement of the spheres on the swimmer's body and on the orientation θ, and E is a constant matrix. Next, denote $F=(f_1 \ldots f_n, \tau_1 \ldots \tau_n)$, where $f_i \in \Re^2$ and $\tau_i \in \Re^2$ are the hydrodynamic force and torque exerted by the fluid on the i^{th} sphere, respectively. A fundamental property of Stokes flow is the existence of a linear relation between forces and velocities, which is given by $F = RU$, where the matrix R, called the *resistance matrix* [4], depends only on the configuration of the spheres, and is typically non-diagonal due to the hydrodynamic interaction between the spheres. Since in general, R cannot be computed exactly, the work in [5] uses the far-field approximation of R which was developed by Swan and Brady [28] for the case of multiple spheres interacting with a plane wall. Finally, denote $F_b=(f_b,\tau_b)$, where $f_b \in \Re^2$ and $\tau_b \in \Re^2$ are the net force and torque acting on the body of the swimmer. It is shown in [5] that F_b satisfies $F_b=T(\theta)^T F$. Since Stokes flow is quasi-steady, the net force and torque on the swimmer's body is zero $F_b=0$. Substituting the relations above, one obtains the relation $\dot{q} = (T^T R T)^{-1} T^T R E u$, which is precisely of the form (1).

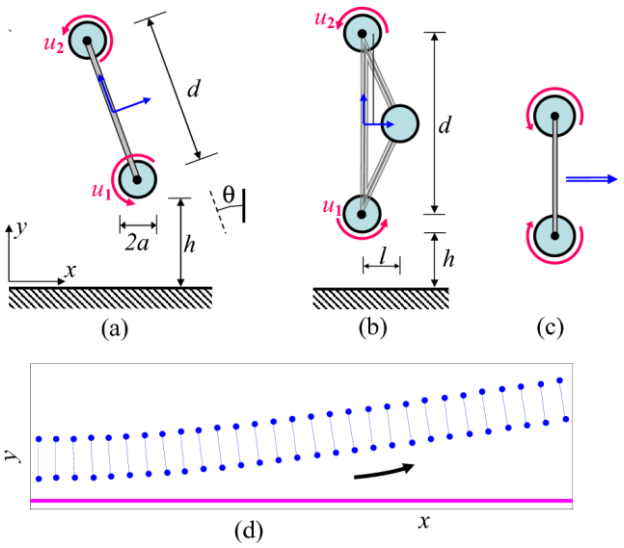

Fig. 1. (a) The two-sphere swimmer. (b) The 2+1-sphere swimmer. (c) The two-sphere swimmer with $u_1 = -u_2$ in unbounded fluid. (d) Snapshots of the two-sphere swimmer with $u_1 = -u_2$ near a wall

B. Geometric Properties of the Equation of Motion

We now review some basic geometric properties of the equation of motion (1) for our system. First, we point out that in the case of unbounded fluid, the system enjoys a special structure called *gauge symmetry*, in which the equation is invariant under rigid-body transformation [15,16]. That is, if we denote v_b as the swimmer's velocity $\dot{q}$ expressed in a body-fixed coordinate frame, then (1) takes the form $v_b=Gu$, where G now is independent of the configuration q. For example, in the two-sphere swimmer with input $u_1=-u_2$, i.e. opposite and equal angular velocities of the spheres, the swimmer moves along a straight line as shown in Fig. 1(c), regardless of its absolute position and orientation. (Note the direction of motion in the figure,

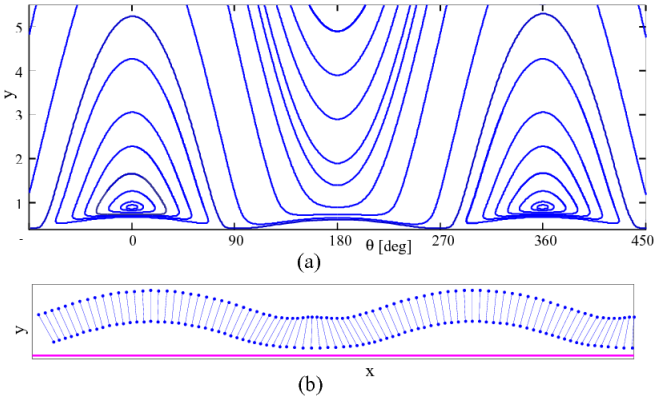

Fig. 2. (a) Phase portrait in (y,θ)-plane for the two-sphere swimmer near a wall under constant input. (b) Snapshots of the swimmer's periodic motion

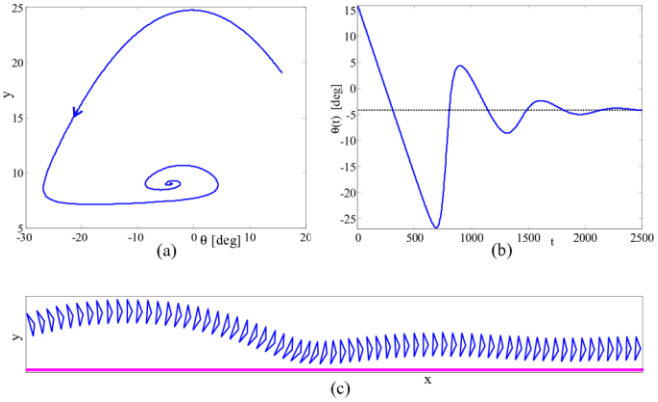

Fig. 3. (a) Phase portrait in (y,θ)-plane for the 2+1-sphere swimmer near a wall under constant input. (b) Time plot of θ(t). (c) Snapshots of the swimmer's motion.

which is just opposite to the one expected intuitively for a large swimmer governed by inertial effects)

However, the presence of the plane boundary destroys the simplifying structure, and under the same input, the swimmer will be repelled from the wall along a curve (Fig. 1(d)). Thus, we focus here on achieving motion of the swimmer *parallel to the wall*, with a fixed orientation and fixed distance from the wall.

In the presence of the wall at y=0, an important observation is that the equation of motion (1) is invariant under translation parallel to the wall, in the x-direction. That is, $G(q)$ in (1) depends only on y and θ, and not on x. The dynamics of y and θ is thus decoupled from that of x. Therefore, if we define $q'=(y,\theta)$, then the dynamics of q' is governed by the equation

$$\dot{q}' = G'(q')u, \qquad (2)$$

where G' is the 2x2 lower submatrix of G in (1). Under this setup, motion parallel to the wall corresponds precisely to *equilibrium solutions* of (2). Formally, such equilibrium points are called *relative equilibria* in the geometric mechanics literature, as they also involve unsteady motion along the x direction. A key step in the study in [5] is the analysis of *stability properties* of these equilibrium points under constant input u, i.e., passive or open-loop stability.

A second important observation in [5] focuses on the case of the two-sphere swimmer, which possesses *fore-aft symmetry*. In this case, the mirror symmetry about θ=0, as well as the linearity of (1) with respect to the input u imply a special structure of (2), called *reversing symmetry*. Under this structure, elements of the first line of $G'(q')$ are even functions of θ, while elements of the second line of $G'(q')$, are odd functions of θ. This implies that for each distance from the wall $y=y_e$, there exists a constant input u_e with a specific ratio u_1/u_2 such that $q'=(y_e,0)$ is an equilibrium point of (2) under the input $u=u_e$, which corresponds to swimming parallel to the wall with a perpendicular orientation θ=0. The reversing symmetry also implies that the linearization of (2) about $(y_e,0)$ has a characteristic polynomial of the form $\Delta(\lambda)=\lambda^2+c$. It is shown in [5] that when y_e is greater than a lower bound, then $c>0$, and $\Delta(\lambda)$ has a pair of imaginary roots. Moreover, in that case $(y_e,0)$ is called *a reversible Lyapunov center* [6], which is a marginally stable equilibrium point enclosed by a continuum of periodic orbits. Fig. 2(a) depicts the phase portrait of trajectories in (y,θ)-plane under a fixed input u_e. Any small initial perturbation about parallel swimming will result in periodic (y,θ)-trajectory, which corresponds to a wave-like motion, as shown in the snapshots in Fig. 2(b).

Finally, [5] studies the case where the swimmer's fore-aft symmetry is slightly broken, as in the case of the 2+1-sphere swimmer of Fig. 1(b). In this case, under a constant input $u=\pm u_e$, there exists an equilibrium point (y_e,θ_e), with a shifted orientation $\theta_e\neq 0$. Moreover, for one of the choices of the sign of u_e, the equilibrium point becomes *asymptotically stable*. As an example, Fig. 3(a) depicts the phase portrait of the 2+1-sphere swimmer under a constant input, and Fig. 3(b) shows time plot of θ(t) converging to its nonzero equilibrium value. Fig. 3(c) shows snapshots of the motion of the swimmer. It can be clearly seen that the swimmer converges passively to steady parallel swimming under an initial perturbation about the equilibrium.

III. Experimental Methods

In this section, we describe the experimental setup which was used in order to demonstrate the theoretical results obtained in [5] with a macro-scale prototype. In order to keep the Reynolds number small in the macro-scaled system, the test fluid was chosen to be highly viscous silicone oil (Polydimethylsil-oxane). The kinematic viscosity of the silicone oil is ν=60,000cSt with specific gravity of 0.976. The near unity value of specific gravity allows for preliminary tests of flotation to be conducted in water.

First, we constructed a swimmer prototype which is propelled by two rotating cylinders submerged in the fluid. The purpose of this system was to confirm theoretical results with a two-sphere model. The experiment was done with nylon cylinders (6.45cm length x 2.54cm diameter) instead of spheres in order to simplify the manufacturing and assembly. Even though the exact interaction of the swimmer

with the fluid is different from the theoretical model, the geometric properties and qualitative results are preserved.

The cylinders are rotated using Micromo 1319SR DC motors connected to a power supply. The angular velocity of each cylinder was proportional to the motor input voltage. In air, the average angular velocity was approximately 60 revolutions per minute at input voltage of 3V. In silicone oil, the average angular velocity was 30 revolutions per minute at 6V. The voltage-velocity ratio was reduced by a factor of four due to the resistance of the viscous fluid. The motors are attached to a wooden frame supported by foam cells floating on the fluid. The goal of the flotation system is to balance gravity and keep the motion of the swimmer two-dimensional in horizontal plane. The fluid is contained in a tank with dimensions of 40cm x 55cm x 30cm. The first swimmer had two pieces of foam for flotation approximately 4.5cm wide and 12cm long. A piece of wood connected the two pieces of foam and acted as support for the entire structure as well as mounts for the motors. The motors were connected to the nylon cylinders and were approximately 7.5cm apart (center to center). The Reynolds number for this swimmer was calculated according to the formula $Re=\omega aL/v$ where ω is the angular velocity, a is the radius of the cylinders and L is the center-to-center distance. Using the values given above, the characteristic Reynolds number is found to be Re=0.017, which justifies the assumption of viscous flow. A picture of the swimmer is shown in Fig. 4 and the dimensions are shown in the sketch in Fig. 5.

The experiments conducted with this swimmer involved motion with the cylinders rotating in equal and opposite angular velocities, as in Fig. 1(c), with input voltages of 3V. In one run, the swimmer was placed in the middle of the tank, far from the walls, to emulate motion in unbounded fluid. The resulting forward velocity was 3.75 mm/sec. In the second run, the swimmer was placed close to one of the walls. The results of these experiments were recorded in movies which can be found in [27]. No quantitative measurements were taken for the experiments involving this model.

Due to the placement of the foam, the first prototype was unable to approach close enough to the wall. A second two-cylinder swimmer was constructed. This second model improved on the first one with a better flotation system that allowed placement of the swimmer closer to the wall. The motor mounting system was improved as well as the rigidity of the overall structure. Reflective markers were added to the system to provide tracking via infrared camera.

An infrared Optitrack Flex V:100 camera was used for tracking. Code was written using the Optitrack SDK in C++ to track two reflective markers attached to the motors. LED's on the camera emit infrared light and the lens picks up the reflection. Suitable objects are determined through programmable threshold variables. These objects are then

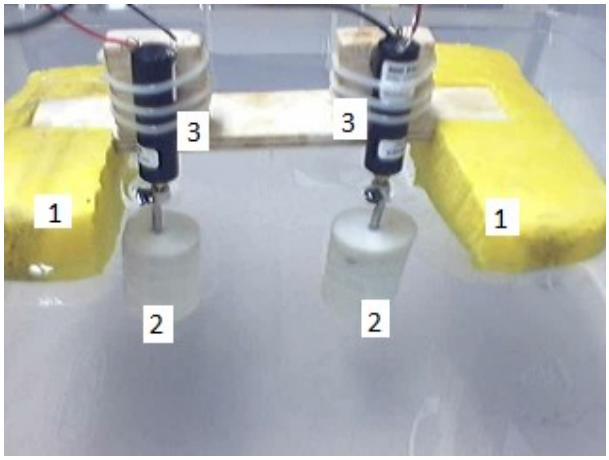

Fig. 4. Picture of first 2-cylinder swimmer. 1. Foam Flotation 2. Nylon Cylinders (2.54cm diameter) 3. Motors

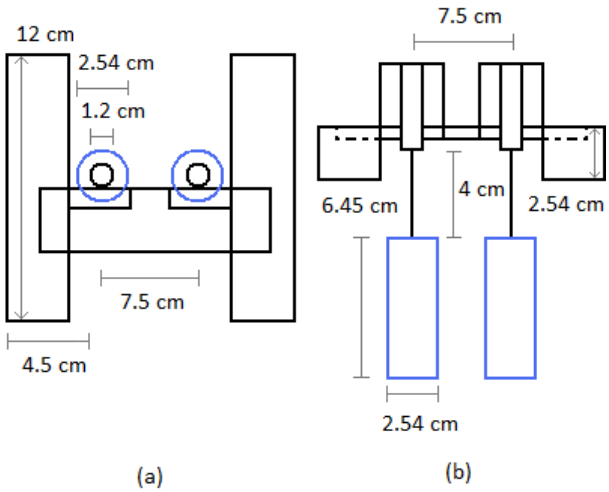

Fig. 5. Sketch of first 2-cylinder swimmer: (a) top view and (b) front view

ranked based on programmable weighting variables. An extensive custom filtering algorithm was written to further erase noise and guarantee tracking of the two desired markers. The output is calibrated against two markers along the wall of the container serving as the reference for the x-axis. The sampling rate of the camera was 100 Hz but due to memory allocation limitations in C++, we took one out of every five data points (20 Hz).

A new tank with dimensions of 110cm x 50cm x 17cm was used for this swimmer. The goal of the longer tank was to better observe the steady state behavior of the swimmer by allowing motion over a longer distance. A picture of the swimmer is shown in Fig. 6 and the dimensions are shown in the sketch in Fig. 7.

Two experiments were conducted with this swimmer near the wall, as follows. In the first experiment, the two cylinders are rotating at equal and opposite angular velocities under input voltages of 6V. In the second experiment, the input voltages for the motor closer to the wall was 5V, while the input voltage to the other motor was 6V, giving unequal

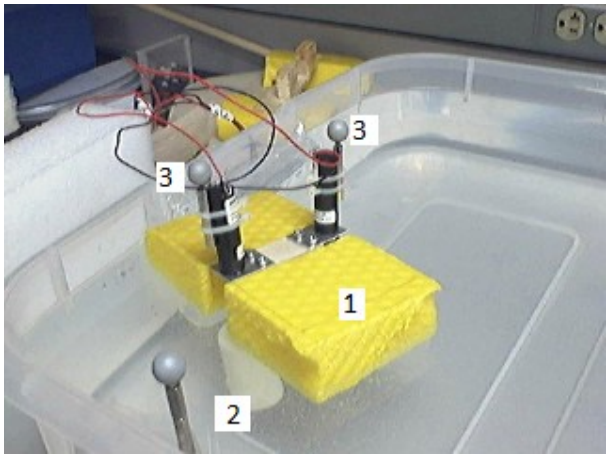

Fig. 6. Picture of second 2-cylinder swimmer. 1. Foam Flotation 2. Nylon Cylinders (2.54cm diameter) 3. Motors / Tracking Markers

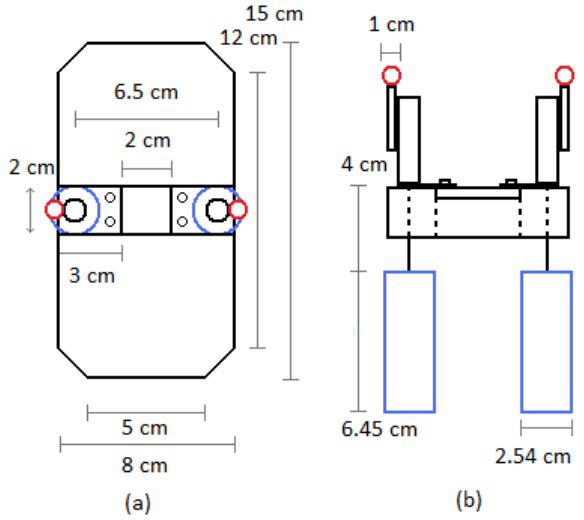

Fig. 7. Sketch of second 2-cylinder swimmer: (a) top view and (b) front view

angular velocities of the cylinders. Measurements from the optical tracking system were recorded for both runs.

In order to demonstrate the theoretical predictions on the 2+1-sphere swimmer, a third swimmer was constructed. This swimmer had further improvements for stability and rigidity with extra supports for the motors to maintain their vertical orientation. A third cylinder with diameter of 1cm was attached rigidly to the front of the swimmer. A picture of this swimmer is shown in Fig. 8 and the dimensions are shown in the sketch in Fig. 9. Experiments conducted with this swimmer include swimming near the wall with input voltages of 6V and 5V, for which the cylinders are rotating at unequal angular velocities, under different initial distances from the wall. The general lab setup with the second tank and cameras are shown in Fig. 10.

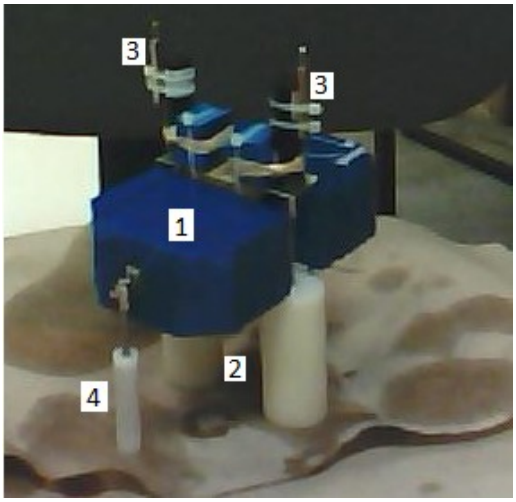

Fig. 8. Picture of third swimmer (2+1-cylinders) 1. Foam Flotation 2. Nylon Cylinders (2.54cm diameter) 3. Motors / Tracking Markers 4. Nylon Cylinder (1cm diameter)

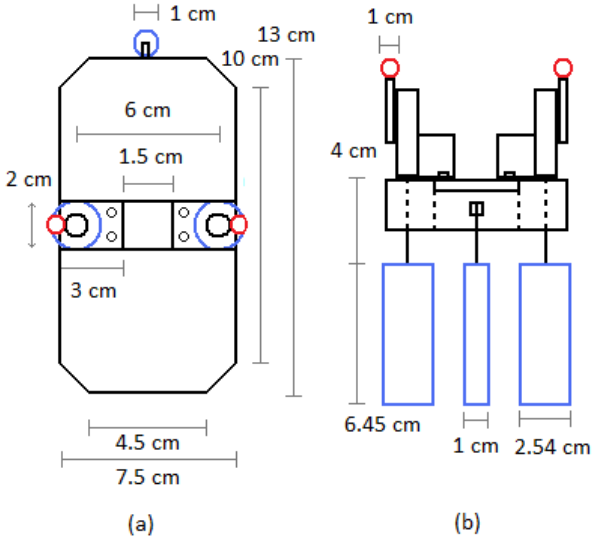

Fig. 9. Sketch of third swimmer (2+1-cylinders): (a) top view and (b) front view

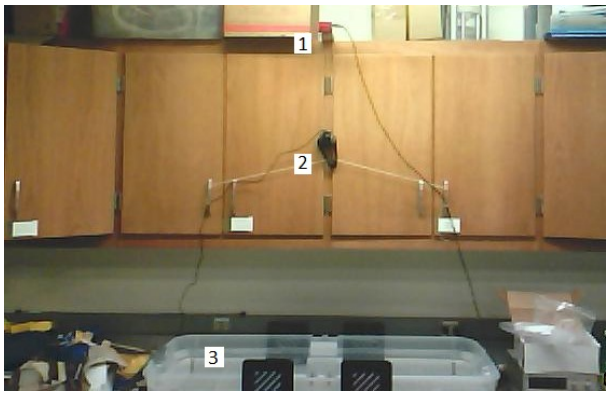

Fig. 10. Final lab setup of the second 2+1-cylinder swimmer, the tracking system, and the video recording system.
1. IR Camera for tracking 2. Webcam for recording video 3. Tank with silicone oil

IV. RESULTS

The experiments with the first prototype of 2-cylinder swimmer under equal and opposite angular velocities were recorded by a webcam, and the movie files are available online at [27]. The results are in qualitative agreement with the theoretical predictions; when the swimmer is placed in the middle of the tank to simulate unbounded fluid, it swims in a straight line. When the swimmer is placed near the wall, it rotates and deviates from the wall, then continues in a straight line when it is sufficiently far from the wall. Using measurements from the tracking system for the second two-cylinder swimmer, Fig. 11 shows snapshots of the motion in the *xy* plane near a wall at y=0 under equal and opposite angular velocities. Fig. 12 shows snapshots of the motion under unequal angular velocities. The result is a nearly periodic motion, as predicted by the theory. Fig. 13 shows phase portrait in (y,θ) plane for the two-cylinder swimmer near the wall under four different initial conditions with constant unequal input voltages. Note that the trajectories are slightly *diverging*, in contrast to the theoretical prediction of perfectly closed orbits as in Fig. 13. Possible reasons for this discrepancy are discussed in the next section. A movie of one representative run with nearly periodic motion can be found in [27].

The raw measurements were noisy. We identified a clear source of the nearly periodic noise signal with frequency ~0.5 Hz, which is precisely the rotation frequency of the cylinders. We believe that the noise is a consequence of some small degree of eccentricity at the shafts and the cylinders caused by the set screws and additional misalignment, which excited slight off-plane motion of lateral oscillations. In order to filter these noises out, all of the measured signals were filtered by a discrete-time low-pass Butterworth filter to eliminate measurement noises. Fig. 14 shows phase portrait in (y,θ) plane for the 2+1-cylinder swimmer near the wall under eight different initial conditions with constant and unequal input voltages. The thick curve in the plot corresponds to a run where y and θ are almost constant, indicating the *existence of a stable equilibrium* of fixed distance from the wall and fixed nonzero angle. A movie of this run is available in [27]. When given an initial perturbation, the theory predicts asymptotic convergence towards the equilibrium point. Our experiments are conducted along a distance which is too short to demonstrate convergence. Nevertheless, using different initial conditions, the phase portrait in Fig. 13 clearly shows a tendency of the trajectories to spiral in towards an equilibrium point, which indicates asymptotic stability, as predicted by the theory and shown in Fig. 3(a).

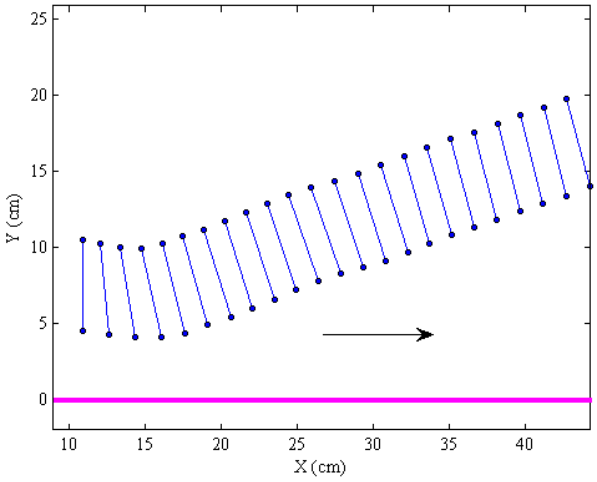

Fig. 11. 2-cylinder swimmer near the wall with equal motor voltages (wall is y=0)

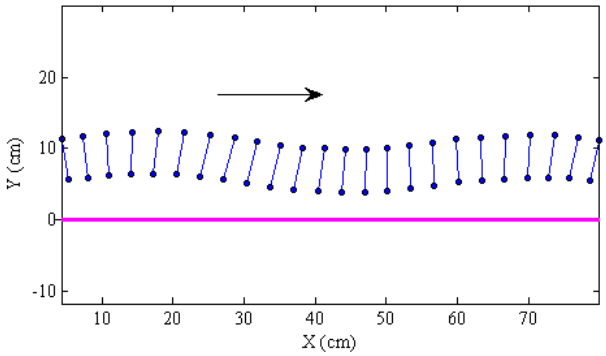

Fig. 12. 2-cylinder swimmer periodic motion near the wall with unequal motor voltages (wall is y=0).

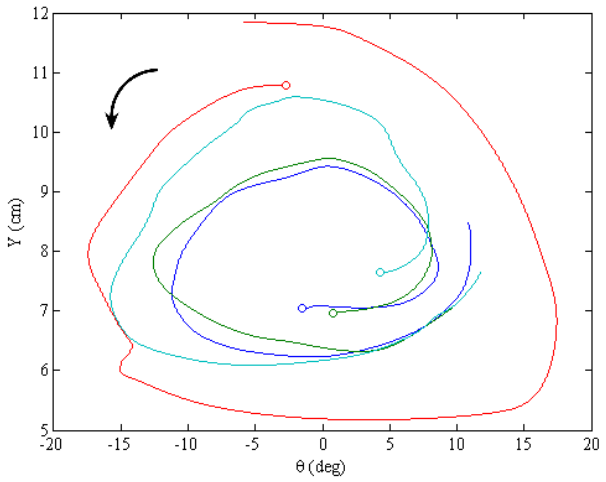

Fig. 13. Phase portraits of experiments with 2-cylinder swimmer. The circles represent the initial positions.

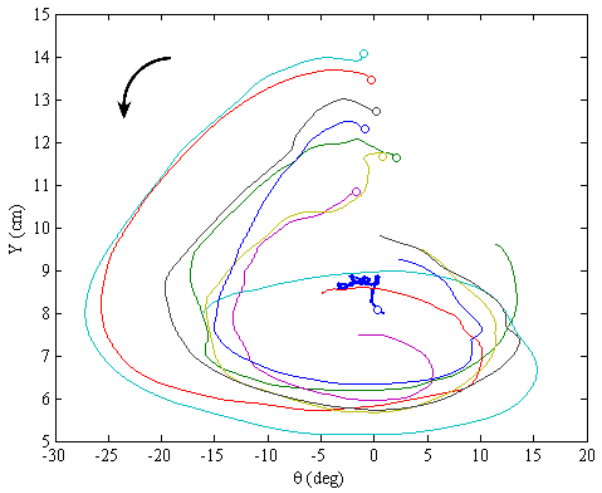

Fig. 14. Phase portraits of experiments with 2+1 cylinder swimmer. The circles represent the initial positions. The thick line corresponds to a run where swimming was near parallel.

V. Discussion

The results display *qualitative agreement* with the behavior predicted in the theory. We now list some discrepancies between the experimental results and the theoretical predictions and suggest possible explanations.

First, note that trajectories of the two-cylinder swimmer with unequal angular velocities in Fig. 13 are slightly *diverging*, in contrast to the theoretical prediction of perfectly closed orbits as shown in Fig. 2(a). A possible explanation is that the exact periodic motion is a consequence of the swimmer being perfectly fore-aft symmetric in the horizontal plane. In the experimental system, misalignment of the flotation structure as well as small off-plane inclination of the swimmer during motion can add some degree of asymmetry which causes the slight divergence.

Second, in some of the trajectories in the phase portrait of Fig. 13 for the 2+1-cylinder swimmer, there is a noticeable transient in the beginning of each run until the trajectory is settled to a spiral curve. This transient can be explained by the duration where the DC power supply develops the desired input voltages once it is initially turned on.

Third, in the phase portraits of Figures 13 and 14 for the 2-cylinder and 2+1-cylinder swimmers, some trajectories are intersecting each other, in contrast to the theoretical prediction shown in Figures 2(a) and 3(a) and to the uniqueness of solutions for planar dynamical systems. This can be explained by unmodelled effects that induce higher-order dynamics, on top of the simple planar system considered in the theoretical model. Examples of such unmodelled effects are off-plane dynamics of the swimmer and inertial effects due to the finite swimmer size.

Other possible sources for discrepancies in the repeatability of runs are associated with the power supply and the DC motors. The assumption that setting input voltages is equivalent to setting velocities is not completely precise due to the unmodelled dynamics of the motor's electric circuit. Moreover, significant heating of the wires was observed during experiments, which may have changed the voltage-velocity ratio and affected the repeatability of the results. Another possible reason for deviation of the actual input voltages from their desired values is the low resolution of the manual voltage control in the DC power supply. Finally, in several experimental runs, we observed events where one of the motors was stuck for a few seconds, possibly due to axis misalignment or internal shaft slippage, which could also explain some of the discrepancies.

Since the two-cylinder swimmer did not produce as many wavelengths as we would have liked due to the physical limitation of the tank length, we now briefly discuss our attempts to make a down scaled swimmer. The behavior of the swimmer scales with the size of the cylinders: the smaller the cylinders, the smaller the wavelength of the periodic motion. We tried to construct smaller swimmers in order to observe more wavelengths in the same tank. The resulting swimmers did not work due to two main reasons. First, the amount of foam required did not scale down very much since we used the same motors, which required roughly the same area of foam for flotation. The submerged nylon cylinders were only slightly denser than the fluid so their effect on flotation is negligible. Second, there was tilting of the swimmer and evolution of off-plane motion near the wall, which led to tipping over of the swimmer or collision with the wall.

VI. Conclusion

In this paper, we reported motion experiments with macro-scale prototypes of low Reynolds number swimmers propelled by rotating cylinders which were supported by a flotation structure. The experiments reproduced the theoretical behavior predicted in our recent work [5]: When the angular velocities of the cylinders were equal, the swimmer diverged away from the wall; When the angular velocities of the cylinders were unequal, periodic motion near the wall was observed; A swimmer with broken fore-aft symmetry demonstrated convergent behavior to asymptotically stable translation parallel to the wall as predicated by the theory. Several attempts to construct a swimmer with smaller cylinders were not successful due to physical limitations and wall collisions caused by the flotation structure.

We now briefly discuss some possible directions for future extensions of the results. First, the finite length of the tank was a key limitation in observing long-distance convergence of the swimmer to a steady state motion. A possible solution is to conduct motion experiments in a circular tank, so that the swimmer can travel over an unlimited distance. This will require adaptation of the theory to circular walls, but analogous symmetry and reversibility arguments will also hold in that case. Second, in order to improve reliability and repeatability of the results, it is possible to add velocity

control that will dictate the input angular velocities directly. This requires adding velocity sensors or encoders at each motor axis, which will affect the weight of the swimmer and the size of the required flotation structure. Third, the model only presented *qualitative* comparison with the theory, since the model in [5] only considers rotating spheres, and accounts for *far-field* interaction with the wall. A development of a more refined theoretical model which will enable *quantitative* comparison with experiments is currently an open problem. Finally, we plan to extend both theory and experiments to shape-changing swimmers, such as the classical example of Purcell's 3-link swimmer [3,9].

ACKNOWLEDGMENTS

S. Z. would like to acknowledge Amir Degani of Carnegie Melon University for his help on the tracking software for the Optitrack Flex V:100 infrared camera and John Van Deusen for his help and work in the Caltech Mechanical Engineering shop.

REFERENCES

[1] E. Lauga and T. R. Powers, "The Hydrodynamics of Swimming micro-organisms", *Rep. Prog. Phys.*, vol. 72, pp. 096601, 2009.

[2] G. Kosa , M. Shoham and M. Zaaroor, "Propulsion Method for Swimming Micro Robots", *IEEE Trans. Robotics*, vol. 23, no. 1, pp. 137-150, 2007.

[3] E. M. Purcell, "Life at Low Reynolds Number", *American Journal of Physics*, vol. 45, pp. 3-11, 1977.

[4] J. Happel and H. Brenner, *Low Reynolds Number Hydrodynamics*, Prentice-Hall, New Jersey, 1965.

[5] Y. Or and R.M. Murray, "Dynamics and Stability of a Class of Low Reynolds Number Swimmers Near a Wall", *Physical Review E,* vol. 79, pp. 045302, 2009.

[6] R. Dreyfus, J. Baudry, M. L. Roper, M. Fermigier, H. A. Stone, and J. Bibette. "Microscopic Artificial Swimmers", *Nature*, vol. 437, pp. 862–865, 2005.

[7] B. Behkam and M. Sitti, "Bacterial Flagella-Based Propulsion and On/Off Motion Control of Microscale Objects," *Applied Physics Letters*, vol. 90, pp. 23902-23904, 2007.

[8] P. Tierno, R. Golestanian, I. Pagonabarraga, and F. Sagues, "Controlled Swimming in Confined Fluids of Magnetically Actuated Colloidal Rotors", *Physical Review Letters*, vol. 101, pp. 218304, 2008.

[9] L. E. Becker, S.A. Koehler, and H. A. Stone, "On Self-Propulsion of Micro-Machines at Low Reynolds Number: Purcell's Three-Link Swimmer", *Journal of Fluid Mechanics*, vol. 490, pp. 15-35, 2003.

[10] J. E. Avron, O Kenneth and D H Oaknin, "Pushmepullyou: An Efficient Micro-Swimmer", *New Journal of Physics*, vol. 7, pp. 234, 2005.

[11] A. Najafi and R. Golestanian, "Simple Swimmer at Low Reynolds Numbers: Three Llinked Spheres", *Physical Review E,* vol. 69, pp. 062901, 2004.

[12] F. Alouges and A. DeSimone and A. Lefebvre, "Optimal Strokes for Low Reynolds Number Swimmers: An Example", *J. Nonlinear Science*, vol. 18, pp. 277–302, 2008.

[13] J. San Martin, T. Takahashi and M. Tucsnak, "A control theoretic approach to the swimming of microscopic organisms", *Quarterly of Applied Mathematics*, vol. 65, no. 3, pp. 405-424, 2007.

[14] J. E. Avron and O. Raz, "A Geometric Theory of Swimming: Purcell's Swimmer and Its Symmetrized Cousin", *New Journal of Physics*, vol. 10, pp. 063016, 2008.

[15] A. Shapere and F. Wilczek, "Geometry of self-propulsion at low Reynolds number", *Journal of Fluid Mechanics*, vol. 198, pp. 557-585, 1989.

[16] S. D. Kelly and R. M. Murray, "Geometric Phase and Robotic Locomotion", *Journal of Robotic Systems*, vol. 12, pp. 417-431, 1995.

[17] J. Koiller and R. Montgomery and K. Ehlers, "Problems and Progress in Microswimming", *J. Nonlinear Science*, vol. 6, pp. 507, 1996.

[18] G. A. de Araujo and J. Koiller, "Self-Propulsion of N-Hinged 'Animats' at Low Reynolds Number", *Qualitative Theory of Dynamical Systems*, vol. 4, pp. 139-167, 2004.

[19] D. F. Katz, "On The Propulsion of Micro-Organisms Near Solid Boundaries", *Journal of Fluid Mechanics*, vol. 64, pp. 33-49, 1974.

[20] G. Zilman, J. Novak and Y. Benayahu, "How do Larvae Attach to a Solid in a Laminar Flow?", *Marine Biology*, vol. 154, pp. 1-26, 2008.

[21] J. Cosson and P. Huitorel and C. Gagnon, "How Spermatozoa Come to be Confined to Surfaces", *Cell Motil. Cytoskeleton*, vol. 54, pp. 56-63, 2003.

[22] L. J. Fauci and A. McDonald, "Sperm Motility in the Presence of Boundaries", *J. Bull. Math. Biol*., vol. 57 no. 5, pp. 679-699, 1995.

[23] M. Ramia, D. L. Tullock and N. Phan-Thien, "The Role of Hydrodynamic Interaction in the Locomotion of Microorganisms", Biophysical Journal, vol. 65 pp. 755-778, 1993.

[24] A. P. Berke, L. Turner, H. C. Berg and E. Lauga, "Hydrodynamic Attraction of Swimming Microorganisms by Surfaces", *Physical Review Letters*, vol. 101, pp. 038102, 2008.

[25] A.M. Leshansky, O. Kenneth, "Surface Tank Treading: Propulsion of Purcell's Toroidal Swimmer", *Physics of Fluids*, vol. 20 issue 6, pp. 063104-06314-14, June 2008.

[26] A. M. Leshansky, O. Kenneth, O. Gat and J. E. Avron, "A Frictionless Microswimmer", *New Journal of Physics*, vol. 9, pp. 145-161, 2007.

[27] Video movies of the experiments are available online at www.technion.ac.il/~izi/research/low_Re_swim/acc2010/

[28] J. W. Swan and J. F. Brady, "Simulation of hydrodynamically interacting particles near a no-slip boundary" *Physics of Fluids*, vol. 19, pp. 113306, 2007.